

Review

Near-Infrared-II Fluorophores for In Vivo Multichannel Biosensing

Feng Ren¹, Tuanwei Li¹, Tingfeng Yao¹, Guangcun Chen^{1,2} , Chunyan Li^{1,2} and Qiangbin Wang^{1,2,*}

¹ CAS Key Laboratory of Nano-Bio Interface, Division of Nanobiomedicine and i-Lab, Suzhou Institute of Nano-Tech and Nano-Bionics, Chinese Academy of Sciences, Suzhou 215123, China; fren2021@sinano.ac.cn (F.R.); twli2020@sinano.ac.cn (T.L.); tfyao2022@sinano.ac.cn (T.Y.); gcchen2011@sinano.ac.cn (G.C.); cyli2012@sinano.ac.cn (C.L.)

² School of Nano-Tech and Nano-Bionics, University of Science and Technology of China, Hefei 230026, China

* Correspondence: qbwang2008@sinano.ac.cn

Abstract: The pathological process involves a range of intrinsic biochemical markers. The detection of multiple biological parameters is imperative for providing precise diagnostic information on diseases. In vivo multichannel fluorescence biosensing facilitates the acquisition of biochemical information at different levels, such as tissue, cellular, and molecular, with rapid feedback, high sensitivity, and high spatiotemporal resolution. Notably, fluorescence imaging in the near-infrared-II (NIR-II) window (950–1700 nm) promises deeper optical penetration depth and diminished interferential autofluorescence compared with imaging in the visible (400–700 nm) and near-infrared-I (NIR-I, 700–950 nm) regions, making it a promising option for in vivo multichannel biosensing toward clinical practice. Furthermore, the use of advanced NIR-II fluorophores supports the development of biosensing with spectra-domain, lifetime-domain, and fluorescence-lifetime modes. This review summarizes the versatile designs and functions of NIR-II fluorophores for in vivo multichannel biosensing in various scenarios, including biological process monitoring, cellular tracking, and pathological analysis. Additionally, the review briefly discusses desirable traits required for the clinical translation of NIR-II fluorophores such as safety, long-wavelength emission, and clear components.

Keywords: NIR-II fluorophore; multichannel biosensing; spectra-domain mode; lifetime-domain mode; fluorescence-lifetime mode



Citation: Ren, F.; Li, T.; Yao, T.; Chen, G.; Li, C.; Wang, Q. Near-Infrared-II Fluorophores for In Vivo Multichannel Biosensing. *Chemosensors* **2023**, *11*, 433. <https://doi.org/10.3390/chemosensors11080433>

Academic Editor: Cynthia M. Dupureur

Received: 28 June 2023

Revised: 20 July 2023

Accepted: 2 August 2023

Published: 4 August 2023



Copyright: © 2023 by the authors. Licensee MDPI, Basel, Switzerland. This article is an open access article distributed under the terms and conditions of the Creative Commons Attribution (CC BY) license (<https://creativecommons.org/licenses/by/4.0/>).

1. Introduction

Fluorescence biosensing is a widely employed technique in the field of life sciences due to its ability to visualize multiplexed physiological and pathological information with rapid feedback, high sensitivity, and high spatiotemporal resolution [1–3]. Multichannel biosensing is particularly significant for the development of biomedicine in both fundamental research and clinical practice [4,5]. It is capable of monitoring multiple processes or quantitatively/qualitatively detecting biomarkers, providing accurate and valuable diagnostic information on tissue, cellular, and molecular features [6,7]. Nevertheless, multichannel fluorescence biosensing in the visible (400–700 nm) and first near-infrared (NIR-I, 700–950 nm) region encounters poor photon penetration depth in mammalian tissues due to the substantial photon scattering/absorption and the interferential autofluorescence (Figure 1a) [8–10]. In contrast, fluorescence imaging in the second near-infrared window (NIR-II, 950–1700 nm) can offer deeper penetration depth and better clarity owing to the suppressed photon scattering ($u \propto \lambda^{-\alpha}$; u : scattering coefficient; λ : wavelength; and α : constant) and reduced tissue autofluorescence (inversely proportional to wavelength) compared with the visible and NIR-I regions (Figure 1b,c) [11–14]. Thus, the advancement of new NIR-II fluorescent probes is necessary to support the development of deep-tissue and multichannel fluorescence biosensing.

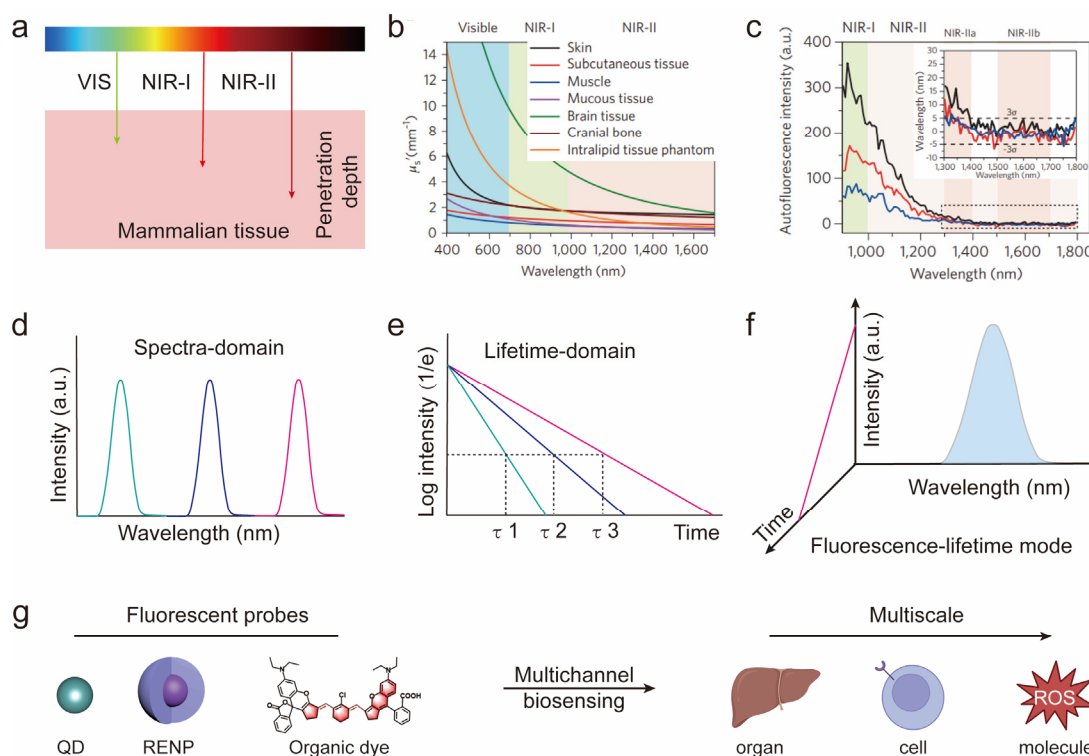


Figure 1. NIR-II fluorophores for deep-tissue multichannel biosensing in versatile modes at a multiscale level: (a–c) light–tissue interactions including tissue penetration depth of light (visible, NIR-I, NIR-II), tissue scattering spectra in 400–1700 nm, and tissue autofluorescence: (a) reproduced with permission from [10], copyright 2020, Wiley-VCH; (b,c) reproduced with permission from [8], copyright 2017, Springer Nature; (d–f) schematic illustration of multichannel biosensing on the spectra-domain, lifetime-domain, fluorescence-lifetime modes; (g) schematic illustration of multiple fluorescent probes (QD, RENP, and organic dye) for biosensing at the multiscale level (organ, cell, molecule).

NIR-II fluorophores, mainly including organic dyes [15,16], quantum dots (QDs) [17,18], and rare-earth-based nanoparticles (RENPs) [19,20], have been developed for multichannel fluorescence imaging using spectra-domain, lifetime-domain, and fluorescence-lifetime modes (Figure 1d–f). The fabrication of these fluorophores, which exhibit nonoverlap emissions–excitations or distinguishable fluorescence lifetimes, is crucial for enabling multichannel biosensing applications [21,22]. To facilitate the qualitative and quantitative analysis of nodules, organic dyes may be designed to control their chemical groups and conjugation units, thereby regulating their fluorescence emissions–excitations and responsiveness to pathological environments [23,24]. QDs may be tuned via the regulation of their size and chemical structure (e.g., core–shell structure and heteroatom doping) to alter their fluorescence emissions [17,25]. RENPs can be modified by doping with various sensitizers/activators and by altering their core–shell structures (e.g., interlayer and shell thickness), resulting in changes in their fluorescence emissions–excitations and lifetimes [19,26]. These fluorescent probes, possessing unique fluorescence and lifetime properties, can be utilized as a versatile toolbox to fulfill the demands of multiscale and multichannel biosensing in a variety of scenarios (Figure 1g).

This review focuses on the advanced development of *in vivo* multichannel biosensing in the NIR-II window for improvement in biomedical diagnostics. We highlight the multifaceted designs and properties of NIR-II fluorophores for *in vivo* multichannel biosensing, which can be utilized in a variety of modes, namely the spectra-domain mode (utilizing cut-off excitation–emission wavelengths), the lifetime-domain mode (using differential fluorescence lifetimes), and the fluorescence-lifetime mode (utilizing the decoding of fluo-

rescence signals via the time-gating technique). We also highlight a selection of their distinctive bioapplication scenarios, including biological process monitoring, cellular tracking, and pathological analysis. Ultimately, we conclude by discussing the merits of multichannel biosensing modes, enabled by the use of versatile NIR-II fluorophores, as well as the outlook for potential challenges and opportunities in multichannel biosensing.

2. Near-Infrared-II Fluorophores

Since the discovery of single-walled carbon nanotubes (SWNTs) with NIR-II fluorescence by the Dai group in 2009 [27], NIR-II fluorophores have flourished. To deploy fluorescence multiplexing for in vivo multichannel biosensing, NIR-II fluorophores demand tunable optical properties in the NIR-II window. Typical fluorophores (QDs, RENPs, and organic dyes) with tunable NIR-II fluorescence are described in subsequent sections.

2.1. QDs

As a class of semiconductor nanocrystals with radii smaller than the excitation Bohr radius, the size and chemical structure of QDs can be easily tailored to tune their fluorescence emission. Lead sulfide (PbS) QDs have size-dependent fluorescence throughout the entire NIR-II region owing to their narrow bandgap and large Bohr radii [28,29]. Bruns et al. designed a series of InAs-based core-shell-structured QDs with narrow and tunable NIR-II emission. Notably, the PLQY (photoluminescence quantum yield) of the core-shell QDs could reach up to 30% in aqueous media compared with PbS QDs (4%) [17]. In addition to shell wrapping, the Wang group reported a cation exchange strategy to boost the PL efficiency of Ag₂E (E = Se and Te) QDs. With the incorporation of gold (Au) atoms into the crystal lattice, alloyed silver gold selenide (AgAuSe) QDs achieved an absolute PLQY of up to 65.3% at 978 nm, and Au:Ag₂Te achieved a calculated PLQY of 6.2% at 1490 nm [11,30]. These versatile NIR-II QDs provide a toolbox for fluorescence multiplexing.

2.2. RENPs

The large quantum numbers of 4f electron configurations provide lanthanide ions (Ln³⁺) with a wealth of optical properties. By simply changing the dopants in RENPs, their emission wavelength can be effectively tuned over the NIR-II region. For instance, Naczynski et al. found that the typical Yb³⁺-sensitized Ln³⁺ (Ln = Er, Ho, Tm, and Pr) in RENPs could produce differential emissions (Ho³⁺: 1185 nm; Pr³⁺: 1310 nm; Tm³⁺: 1475 nm; and Er³⁺: 1525 nm) after absorbing 980 nm photons [31]. In comparison, for a system highly doped with Er³⁺, RENPs possess multiwavelength excitations (980 nm, 808 nm, and 658 nm) and NIR-II emission (1550 nm) after inert shell coating to alleviate surface and concentration quenching effect [32]. In addition to the tunable multiwavelength excitation-emission, the long luminescence lifetime is also one of the intrinsic properties of RENPs. Tailoring the structural parameters of core-shell RENPs, including the concentrations of dopants, the thicknesses of interlayer and inert shell and the crystal phase of host matrixes could effectively tune the NIR-II lifetime of Ln³⁺ activators with different proportions [33]. These feasible pathways to achieve NIR-II RENPs with highly distinguishable fluorescence wavelengths and lifetimes favor the development of advanced multiplexing modes.

2.3. Organic Dyes

Organic dyes with NIR-II fluorescence have been synthesized based on cyanine dyes (D- π -A) or donor-acceptor-donor (D-A-D) structures by tailoring their chemical groups or conjugation units. Cyanine dyes typically consist of two heterocyclic end groups connected by a length-tunable polymethine chain [34]. Lengthening the polymethine chain or modifying heterocycle can endow cyanine dyes (Flav7, IR-1061, IR-26, and FD-1080) with tunable NIR-II fluorescence by enhancing the π -conjugate strength [35,36]. The first NIR-II organic dye based on the D-A-D structure, CH1055, was reported by the Dai group, which is composed of a benzobisthiazole acceptor and a triphenylamine donor [37].

Although organic dyes generally face the problem of aggregation-caused quenching (ACQ) in biological environments, mainly due to the strong intramolecular π - π interactions [38], Tang et al. have discovered and explored a type of luminogens with aggregation-induced emissions (AIEgens) since 2001 [39,40]. Tailoring the electron donors (D) and electron acceptors (A) of AIEgens can extend their emissions to the NIR-II window, such as D-A-structured 2TT-oC26B molecules [41,42]. More prominently, AIEgens are capable of multiphoton absorption, enabling multiphoton fluorescence bioimaging to decipher deep-tissue biological structures via NIR-II excitation [43–45]. Typical approaches such as tailoring D-A structures and expanding the conjugation length could enhance the multiphoton absorption cross-sections of AIEgens [46]. In addition, the highly ordered assembly of organic dyes provides an effective avenue to achieve longer wavelengths beyond 1500 nm. J-aggregates with head–tail molecular stacking of organic dyes resulted in strong red-shifted absorption–emission (approximately 300 nm) and boosted fluorescence intensity of FD-1080 compared with that of the dye monomer [14]. These versatile approaches to obtaining NIR-II organic dyes with brightness and differential excitation–emission wavelengths are beneficial for the development of fluorescence multiplexing methods.

3. Spectra-Domain Multichannel Biosensing

The implementation of *in vivo* multichannel fluorescence biosensing requires a meticulous selection of nonoverlap excitation–emission wavelengths for the use of NIR-II fluorophores. To achieve simultaneous visualization/tracking of multiple analytes at the tissue or cellular level, fluorophores with varying excitation–emission properties are necessary to bind specific targets. On the other hand, in order to quantitatively measure analytes at the molecular level, ratiometric fluorophores with multiple excitation–emission wavelengths are typically required to enable selective responsiveness. The rational designs and bioapplications of these NIR-II fluorophores will be elucidated in-depth in subsequent sections.

3.1. Excitation–Emission Multiplexed Biosensing

In order to facilitate the visualization of multiple pathological or physiological parameters at the tissue or cellular level, it is essential to use fluorophores with nonoverlap excitation–emission spectra that enable to simultaneously tag and visualize them in the NIR-II imaging window (Figure 2a,b). Recently, Cosco et al. tuned the absorption properties of flavylum polymethine dyes utilizing flavylum heterocycles, which allowed for the real-time excitation multiplexing of living mice at the tissue level using NIR-II emitters (MeOFlav7: 980 nm excitation; JuloFlav7: 1064 nm excitation) [36]. However, the long-term retention of these molecules has the potential to induce toxicity in major organs. To overcome this limitation, Yao et al. designed a series of highly efficient renal clearance and long blood circulation aza-boron-dipyrromethene (aza-BODIPY) NIR-II macromolecular fluorophores (FBP790: 730 nm excitation, 950 nm long-pass optical filter; FBP1025: 980 nm excitation, 1200 nm long-pass optical filter) and applied them for excitation multiplexed imaging of tumors and surrounding vessels [47]. Nevertheless, these NIR-II organic fluorophores are restricted to the emission wavelength range of 1000–1500 nm, thereby limiting their utility in achieving high-resolution NIR-IIb fluorescence imaging (1500–1700 nm) with millimeter-scale penetration depth and micron-level resolution [48–50]. Although AIEgens (DCBT dots) with multiphoton absorption could obtain fine structures of brain vasculatures of mice and macaque by using three-photon fluorescence bioimaging with NIR-IIb excitations (1550 nm), their progress in the field of excitation–emission multiplexed biosensing remains sluggish [51–53].

To date, only a handful of NIR-IIb fluorophores have been developed for multichannel fluorescence biosensing, including rare-earth-based nanoprobe and colloidal QDs [54,55]. Given the intrinsic location of 4f energy levels of lanthanides, Er(III) is the mainstream activator generating NIR-IIb emission (around 1530 nm) under varied excitation sources (650 nm, 808 nm, and 980 nm) [32,56–58]. To expand the range of small-molecule lanthanide

complexes for biosensing, Wang et al. developed a hybrid Er(III)-bacteriochlorin complex (EB766) with 760 nm excitation and bright luminescence at 1530 nm [59]. Compared with typical co-doped lanthanide nanoparticles (ErNPs: NaYF₄:20%Yb,2%Er@NaYF₄), the nonoverlap excitations of EB766 (760 nm) and ErNPs (980 nm) facilitate robust NIR-IIb multiplexed biosensing for deciphering multiple tissue structures (such as lymph nodes and lymph vessels in jaw and footpads) with superior signal-to-background ratios (SNRs: 3.92–22.79) (Figure 2c). Alongside lanthanides, colloidal QDs, such as PbS QDs with a narrow bandgap and large Bohr radius, offer tunable emission coverage of the NIR-II region via size control [60,61]. By synthesizing NIR-IIa and NIR-IIb fluorescent PbS/CdS core-shell QDs functionalized with Gr-1 and CD-1b antibodies, respectively, Yu et al. exploited this emission multiplexing strategy for in vivo colocalization of myeloid-derived suppressor cells (MDSCs). By connecting the unique emission properties of these QDs to the targeted MDSCs, this approach holds significant potential for enhancing immunotherapy (Figure 2d) [21]. Overall, these results demonstrate that the excitation–emission multiplexing approach is highly suitable for a real-time diagnosis of tissue lesions and therapeutic feedback at the cellular level.

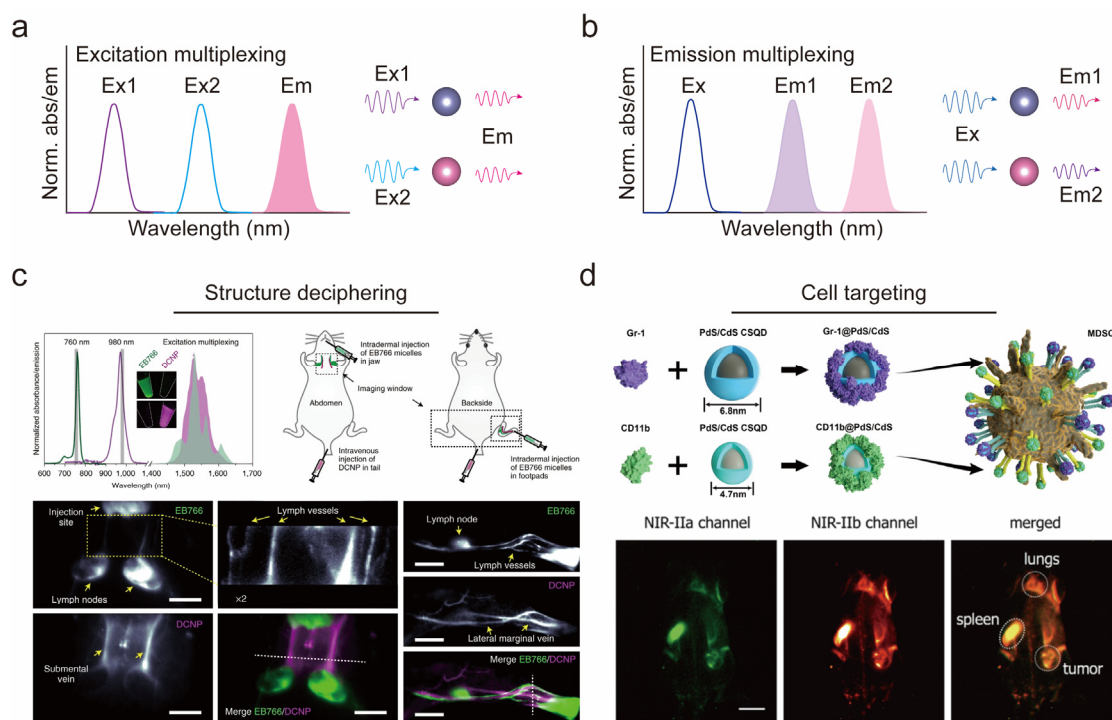


Figure 2. Excitation–emission multiplexed biosensing: (a,b) schematic illustration of NIR-II fluorophores enabled excitation–emission multiplexing; (c) excitation multiplexing biosensing to decipher multiple tissues of living mice using NIR-IIb lanthanide-based probes (EB766: 760 nm excitation, 1530 nm emission; DCNP: 980 nm excitation, 1530 nm emission). Reproduced with permission from [59], copyright 2021, Springer Nature; (d) emission multiplexing to target MDSCs using size-varied PbS/CdS QDs. Reproduced with permission from [21], copyright 2019, American Chemical Society.

3.2. Ratiometric Fluorescence Biosensing

In addition to multichannel biosensing utilizing multiple fluorophores, fluorophores with the capacity to emit or excite at different wavelengths have the potential to enable the quantitative measurement of pathological parameters at the molecular level. For this purpose, the fluorophores must possess an emission–excitation pattern that responds solely to the analyte (such as reactive oxygen species, enzymes, and pH), while the other remains inert and acts as a reference signal (Figure 3a,b). To achieve this, Lan et al. designed

a series of responsive NIR-II probes (enzyme-responsive Rap-N, ROS-responsive Rap-R, and pH-responsive Py-H; ratiometric emission: 945 nm/1010 nm) based on the Py-2 molecular platform for ratiometric fluorescence biosensing [24]. These single-component NIR-II dyes have the potential to selectively visualize and quantitatively measure enzymes and small molecules in living mice with significant ratiometric fluorescence signals (F1900LP/F1100LP). Additionally, NIR-II organic nanosensors for ratiometric fluorescence imaging can be designed based on intramolecular Förster resonance energy transfer (FRET). To create the NIR-II ratiometric fluorescent dyes, Yu et al. covalently linked an asymmetric aza-BODIPY with an ONOO⁻-responsive meso-thiocyanine, known as the aBOP-IR1110 (ratiometric emission: 950 nm/1110 nm). This process results in ONOO⁻-altered intramolecular FRET, which generates a linear ratiometric response (F1950LP/F1100LP) [62]. The aBOP-IR1110 can withstand biological media, thereby preventing spectral shift and distortion and facilitating the dynamic monitoring of oxidative stress in traumatic brain injury and evaluating therapeutic efficiency with high in vivo sensing accuracy. However, the currently available organic ratiometric fluorophores have a limited emission wavelength that falls short of 1500 nm, along with a small Stokes shift, thereby limiting their usability in deep-tissue biosensing.

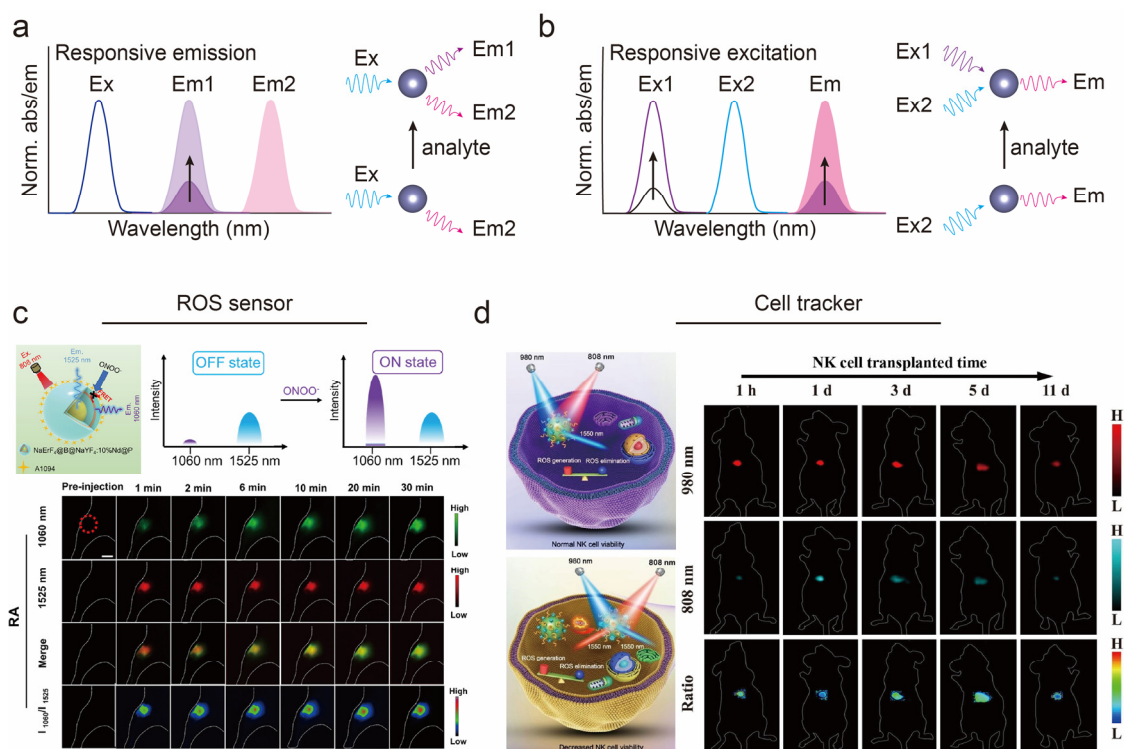


Figure 3. Ratiometric fluorescence biosensing: (a,b) schematic illustration of NIR-II fluorescent nanocomposites enabled ratiometric fluorescence biosensing; (c) emission-responsive NIR-II hybrid nanosensor for ratiometric fluorescence imaging of inflammation using A1094-RENPs hybrid nanosensor. Reproduced with permission from [63], copyright 2022, American Chemical Society; (d) excitation-responsive NIR-II hybrid nanosensor for ratiometric fluorescence imaging of NK cell viability using IR780-RENPs hybrid nanosensor. Reproduced with permission from [64], copyright 2021, Wiley-VCH.

Hybrid ratiometric nanosensors offer a variety of options for emission wavelength and responsive substances, thus enabling quantitative in vivo biosensing. Sun et al. developed a NIR-II ratiometric nanocomposite by coupling the dual-emission (1060 nm and 1525 nm) RENPs (NaErF₄@NaYF₄@NaYF₄:10%Nd@NaYF₄) with ONOO⁻-responsive A1094 organic dyes (absorbance:1094 nm). The FRET between them allowed for the rapid and sensitive

in vivo detection of ONOO⁻ levels (Figure 3c) [63]. Since ROS/RNS levels are highly correlated with the activation and viability of immune cells, in vivo molecular analysis can provide valuable feedback during cancer immunotherapy [65,66]. Liao et al. developed a NIR-II ratiometric nanocomposite by coating dual-excitation (ex: 808 nm and 980 nm; em: 1525 nm) RENPs with IR786 dyes. The degradation of ROS-responsive dyes solely activates the 808 nm excitation channel through the absorption competition-induced emission effect (ACIE) [64]. Therefore, the hybrid nanosensor can evaluate the cell viability of natural killer (NK) cells by measuring the excess generation of ROS, while simultaneously tracking the NK cells via the stable signal excited at 980 nm (Figure 3d). Such intracellular ROS-induced ratiometric NIR-II fluorescence biosensing has the potential to pave the way for in vivo companion diagnostics in cancer immunotherapy.

3.3. Spectra-Domain Multichannel Biosensing in Various Scenarios

In the field of oncology, mapping the heterogeneity of primary and metastatic tumors is vital for precision medicine [4]. Detecting the metastasis of cancer cells and the migration of immune cells is essential from a fundamental research perspective, as it can help identify the most effective therapies [67,68]. To study cellular behavior in live animals, intravital microscopic multiplexing is essential [69]. Wang et al. developed a cell tracking probe (CT1530) for intracellular delivery, comprising the cell-penetrating peptide HIV-TAT-conjugated EB766–bovine serum albumin (BSA) complex [59]. Using fluorescence signals (green, 1100–1300 nm) from Cy7.5 phospholipid micelles to highlight the cerebrovascular system, the researchers found that cancer cells were arrested in vessel bifurcations through physical occlusion via the nonoverlap fluorescence (red, 1400–1600 nm) from CT1530-labeled 143B cells (Figure 4a). On the other hand, evaluating the infiltration of immune cells into tumors is crucial for determining therapeutic efficacy. Hao et al. developed a NIR-II emission multiplexing strategy to visualize the recruitment of NK cells into the tumor via the programmable administration of Ag₂Se-QD-based nanodrug (em: 1350 nm) containing SDF-1 α (stromal-cell-derived factor-1 α , the chemokine of NK-92 cells) and Tat-Ag₂S QDs-labeled NK-92 cells (em: 1050 nm) (Figure 4b) [70]. This multichannel biosensing strategy has significant implications not only for precision medicine but also for individual therapeutic schedules and companion diagnostics [4,71]

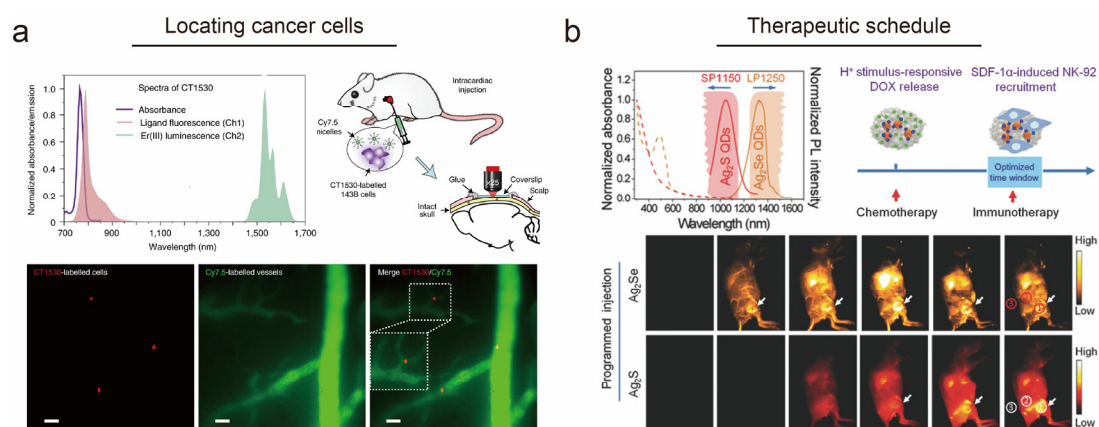


Figure 4. Cont.

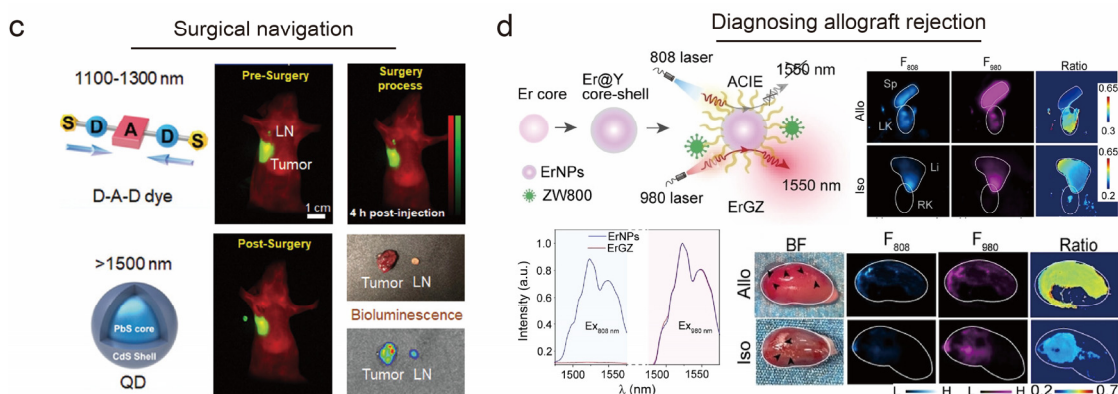


Figure 4. Spectra-domain multichannel biosensing in versatile scenarios: (a) intravital multiplexed imaging of cancer cell metastases in mouse brain. Reproduced with permission from [59], copyright 2021, Springer Nature; (b) NIR-II fluorescence multiplexed imaging to program the chemotherapy and immunotherapy against breast cancer. Reproduced with permission from [70], copyright 2018, Wiley-VCH; (c) NIR-II emission multiplexing imaging for surgical navigation using QDs and D-A-D dye. Reproduced with permission from [72], copyright 2020, Wiley-VCH; (d) NIR-IIb ratiometric imaging for allograft rejection diagnosis using granzyme-B-responsive ErGZ nanosensor. Reproduced with permission from [73], copyright 2023, Wiley-VCH.

In clinical practice, a first-in-human study has demonstrated the potential of intraoperative NIR-II fluorescence imaging in guiding liver tumor surgery [5]. In addition to primary tumors theranostics, detecting and monitoring cancer metastasis is critical for tumor staging, therapeutic decision making, and prognosis. For instance, in the case of breast cancer, multiorgan metastasis often leads to a median survival rate of fewer than two years for patients. Lymph nodes (LNs) are frequently the primary site of tumor cell dissemination, which can disrupt the immune microenvironment [74]. To enable precise surgical resection, Tian et al. developed an emission multiplexing approach that simultaneously labels the metastatic tumor (IR-FD dye) and tumor metastatic proximal LNs (PbS/CdS QDs) (Figure 4c) [72]. Meanwhile, diagnosing allograft rejection to improve the immune management of transplant recipients in the early stages is also essential, as transplantation can cause severe postoperative complications [75,76]. Chen et al. developed a responsive NIR-II fluorescent nanosensor by linking ErNPs ($\text{NaErF}_4@ \text{NaYF}_4$: 980/808 nm excitation; 1550 nm emission) with ZW800 dye, allowing for the ratiometric biosensing of granzyme B, which is overexpressed in recipients' T cells during the onset of allograft rejection, in contrast to the gold-standard biopsy (Figure 4d) [73]. This strategy could also be applied to in situ monitoring of tissue regeneration. Pei et al. integrated 3D-printed bioactive glass scaffolds with a responsive NIR-II fluorescent nanosensor, enabling in situ monitoring of early inflammation, angiogenesis, and implant degradation during mouse skull repair [77]. These results illustrate the potential of spectral-domain fluorescence multiplexing in clinical translation.

4. Lifetime-Domain Multichannel Biosensing

As fluorescence imaging involves real-time light irradiation, it inevitably leads to tissue scattering and autofluorescence. However, the use of cut-off wavelengths allows for fluorescence multiplexing through optical filters, while simultaneously filtering out scattering light. Although tissue autofluorescence is significantly attenuated in the NIR-II region, this often compromises the contrast and sensitivity of fluorescence imaging [78,79]. To achieve background-free multiplexed imaging, manipulating the fluorescence lifetime of fluorophores matters. Fluorophores with longer lifetimes than tissue autofluorescence (0.1–5 ns) can provide a luminescence signal even after the laser is turned off (Figure 5a) [9,80]. This time-gating technique can eliminate interference from the excitation light to improve the contrast of fluorescence imaging [81]. To enable this lifetime-domain

multichannel biosensing, it is essential that the fluorophores have a tunable lifetime distinct from that of tissue autofluorescence, which is mainly limited to RENPs, known as t-dots (Figure 5b).

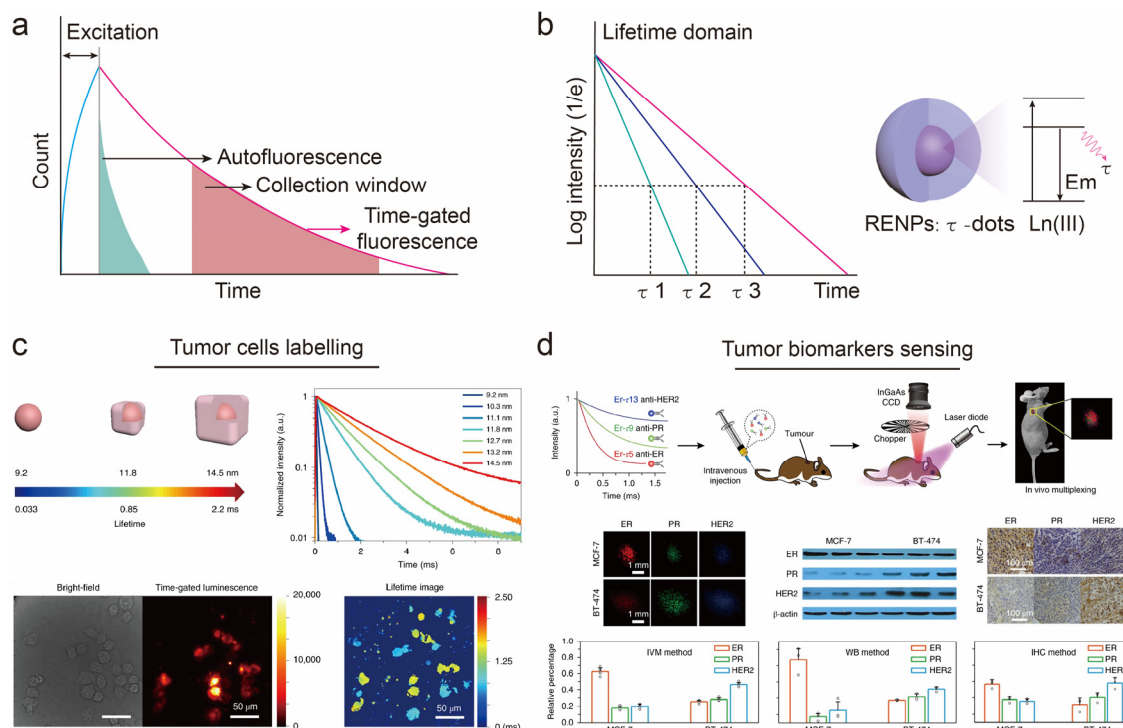


Figure 5. Lifetime-domain multichannel biosensing: (a) fluorophores with long lifetimes enable background-free fluorescence imaging through time-gated gear; (b) schematic illustration of fluorescence-lifetime-tunable RENPs; (c) fluorescence-lifetime-tunable $\text{NaYbF}_4@CaF_2$ by modulating shell thickness for tagging HeLa cells. Reproduced with permission from [82], copyright 2019, Springer Nature; (d) lifetime-engineered ErNPs with versatile antibodies (ER, PR, and HER2) binding for in vivo lifetime-domain multiplexing to identify tumor subtype in living mice. Reproduced with permission from [33], copyright 2018, Springer Nature.

RENPs boast a flexible fluorescence lifetime ranging from microseconds to milliseconds, which can be easily tuned based on various structural parameters such as dopants, their concentrations, and relay–inert layer thickness [83–85]. Gu et al. achieved a highly efficient conversion of pulsed excitation into long-decaying NIR luminescence without energy loss by using a NIR light transducer ($\text{NaYbF}_4@CaF_2$ core–shell RENPs) [82]. The optically inert CaF_2 shell encapsulating the Yb(III) signal transducers allowed for the tunable lifetime of RENPs spanning from 0.033 to 2.2 ms (emission: 980 nm) by adjusting the shell thickness (Figure 5c). Unlike fluorescence imaging, lifetime-domain multichannel imaging demonstrated the ability to distinguish two different types of nanoparticles with unique lifetimes (0.84 and 1.45 ms, respectively) utilized for labeling HeLa cells (Figure 5c). Meanwhile, Fan et al. systematically modulated the energy relay in ErNPs (Er-doped RENPs) to enable fluorescence imaging with tunable lifetimes, spanning three orders of magnitude (from microseconds to milliseconds) with 1525 nm emission [33]. Moreover, by conjugating lifetime-discriminating ErNPs (Er- τ 5, Er- τ 9, and Er- τ 13) with antibodies that target various breast cancer receptors, including estrogen receptor (ER), progesterone receptor (PR), and human epidermal growth factor receptor 2 (HER2), in vivo fluorescence-lifetime multiplexing was utilized to identify the precise tumor subtypes in living mice (Figure 5d).

5. Fluorescence-Lifetime Multichannel Biosensing

Spectra-domain multiplexing is often hindered by errors in penetration depth that arise from wavelength variations, and lifetime-domain multiplexing lacks the ability to acquire fluorescence signals in real time during imaging because of the time-consuming fluorescence signal acquisition protocol [86]. Nevertheless, the flexibility of alternating between these two fluorescence imaging modes offers a groundbreaking solution to overcome the limitations of each technique. In the fluorescence channel, emissions with the same wavelength can be distinguished via a time-resolved method or dynamic variations in fluorescence intensity can be detected. In comparison, in the lifetime channel, the time-gating technique acquires delayed luminescence signals accordingly. By seamlessly integrating these imaging channels, we can visualize pathological environments in real time without any penetration-depth errors. This cutting-edge strategy unlocks new prospects for the advancement of multichannel biosensing applications.

Immunotherapy is a pivotal treatment for malignant tumors that has demonstrated significant clinical outcomes. However, it still faces several formidable challenges, including low response rates and immune-related adverse events [87,88]. Therefore, predicting and monitoring the therapeutic response to immunotherapy is of paramount importance to achieve better patient outcomes [89,90]. Since dual emission with the same wavelength can be separated by the time-gating technique to allow for the colocalization of multiple targets, avoiding the penetration-depth error (Figure 6a) [86], Zhong et al. developed a two-plex NIR-IIb imaging approach for *in vivo* visualization of immune responses using long-lived ErNPs-aPDL1 (lifetime: 4.2 ms) to tag tumor cells and short-lived PbS-aCD8 QDs (lifetime: 46 μ s) to tag CD8⁺ T cells, respectively (Figure 6b) [91]. The infiltration of CD8⁺ T cells could be visualized instantly, which is promising for predicting the extent of immune activation [92]. Therefore, this approach could serve as a companion diagnostic for immunotherapy in clinical practice [71].

In contrast to dual-NIR-IIb emission at the same wavelength, the coherent recovery of fluorescence and lifetime allows for real-time *in vivo* localization and measurement through two channels at the same penetration depth (Figure 6c). Zhao et al. devised a TME (tumor microenvironment) nanosensor for hepatocellular carcinoma (HCC) detection by using β -NaYF₄@NaYF₄:1%Nd NPs and MY-1057 cyanine dyes, which respond to ONOO⁻-induced variation in FRET between them (Figure 6d) [79]. Furthermore, the authors developed a luminescence resonance energy transfer (LRET) toolbox consisting of amorphous manganese oxide (MnO_x) and versatile lanthanide nanoparticles for quantifying intratumor glutathione (GSH) levels *in vivo* [93]. The results of a blind study showed that the quantified intratumor GSH levels of different types of tumors were highly consistent with the commercial kit results. In addition to the hybrid nanosensor, Chang et al. prepared a novel glutathione-capped copper–indium–selenium (CISE) nanotube with a NIR-II emission (1010–1130 nm) for phosphorescence imaging [94]. Notably, phosphorescence is a type of photoluminescence related to fluorescence that is featured with long-lived luminescence and large Stokes shifts. Unlike dual-channel signal recovery, CISE nanotubes have the unique ability to self-assemble in an acidic physiological environment (pH: 5.5–6.5) and switch from short-lived fluorescence to phosphorescence, allowing for the precise and accurate identification of tumor lesions through fluorescence-lifetime dual-channel imaging. (Figure 7). These results strongly indicate that a logical switch between imaging modes based on fluorescence and lifetime channels holds great promise for *in vivo*, real-time identification and quantification of a wide range of biomarkers.

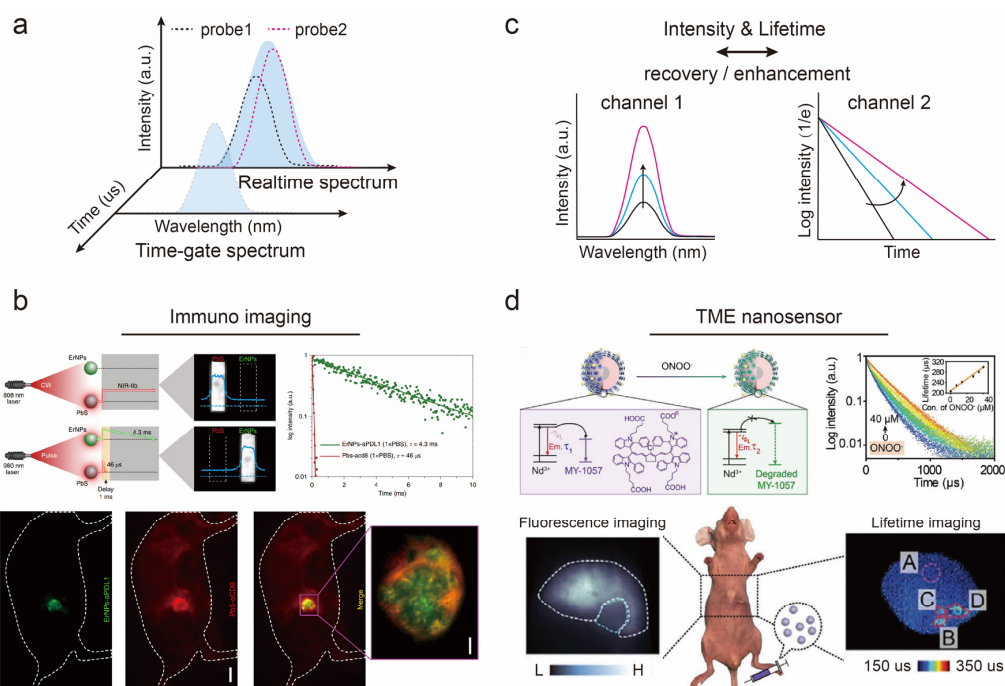


Figure 6. Fluorescence-lifetime multichannel biosensing: (a) schematic diagram of NIR-II signals separation through time-resolved technique; (b) NIR-II fluorescence-lifetime dual-channel imaging for monitoring immunotherapy using ErNPs (em:980 nm; ex: 1530 nm) and PbS/CdS QDs (em: 808/980 nm; em: 1600 nm). Reproduced with permission from [91], copyright 2019, Springer Nature; (c) schematic illustration of a responsive nanosensor with luminescence-lifetime synergistic recovery; (d) TME responsive (ONOO^-) nanosensor (DCNPs@MY-1057) with luminescence-lifetime dual-channel imaging for HCC liver tumor diagnosis. Reproduced with permission from [79], copyright 2020, Wiley-VCH.

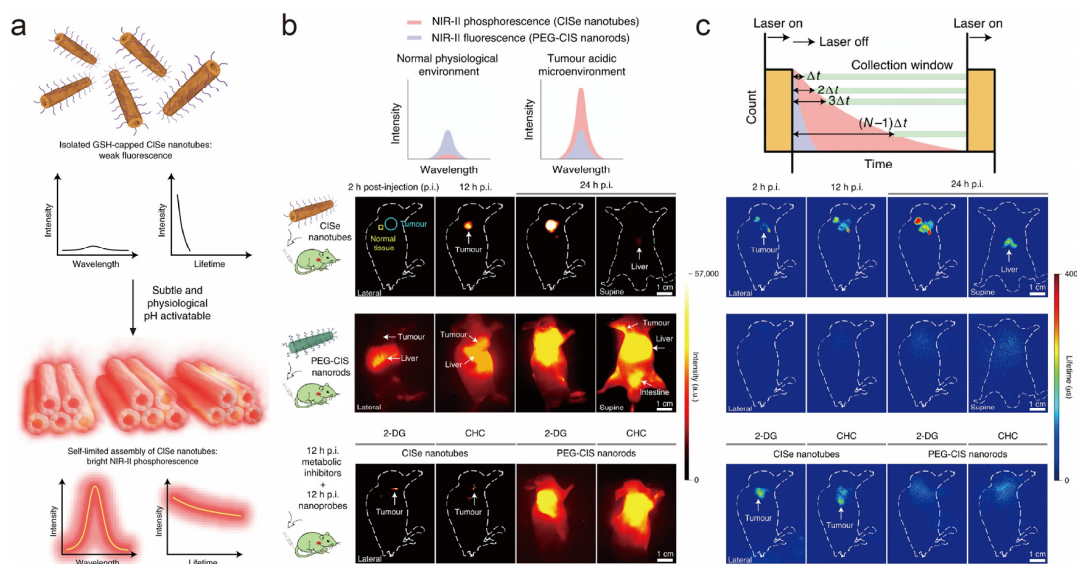


Figure 7. CISe nanotubes as a pH-responsive NIR-II phosphorescent probe for fluorescence-lifetime biosensing: (a) schematic illustration of emission and lifetime enhancement of CISe NIR-II phosphorescent probe upon pH responsiveness; (b) NIR-II fluorescence imaging and (c) time-resolved NIR-II imaging of living mice bearing 143B osteosarcoma cancer xenografts after intravenous administration of CISe nanotubes or PEG-CIS nanorods (dosage: 20 mg kg^{-1}). Reproduced with permission from [94], copyright 2021, Springer Nature.

6. Conclusions and Outlook

In conclusion, this review provides an overview of NIR-II fluorophores for multichannel fluorescence biosensing in two sections: imaging modes and biosensing applications. Based on the current development of NIR-II fluorophores, we divided multichannel biosensing into spectra-domain, lifetime-domain, and fluorescence-lifetime modes, and discussed their respective application scenarios (Table 1). With their respective merits, they can be applied in diverse scenarios. In vivo spectra-domain multiplexing can visualize pathological processes in real time; lifetime-domain multiplexing can pinpoint multiple targets with higher contrast; and fluorescence-lifetime multichannel biosensing can provide real-time and high-contrast imaging results. Multichannel NIR-II fluorescence biosensing is promising for noninvasive in vivo diagnosis with precision. Despite these impressive developments in multichannel fluorescence biosensing with the use of advanced NIR-II fluorophores, some fields are still worth exploring for their application in clinical practice.

Table 1. Summary of NIR-II fluorophores for multichannel biosensing.

NIR-II Sensor	Ex. (nm)	Em. (nm)	Mode	Application	Ref
Er(III)-bacteriochlorin complexes	766	1530	Spectra domain	Multiplexing of tissues and tumor cells	[59]
PbS/CdS QDs	808	1100&1600	Spectra domain	Multiplexing of MDSCs	[21]
NaErF ₄ @NaYF ₄ @NaYF ₄ :10%Nd@NaYF ₄ @A1094	808	1060&1525	Spectra domain	Ratiometric imaging of RNS	[63]
DCNP@IR760s	808&980	1550	Spectra domain	Ratiometric imaging of ROS to track NK cell viability	[64]
Ag ₂ S&Ag ₂ Se QDs	808	1050&1350	Spectra domain	Multiplexing-guided therapeutic schedule	[70]
PbS/CdS QDs & IR-FD dye	808	1100&1600	Spectra domain	Multiplexing-guided surgical navigation	[72]
NaErF ₄ @NaYF ₄ @ZW800	808&980	1550	Spectra domain	Ratiometric imaging of GzB to diagnose allograft rejection	[73]
NaYbF ₄ @CaF ₂	920	980	Lifetime domain	Tumor cells labeling	[82]
NaGdF ₄ @NaGdF ₄ :Yb,Er@NaYF ₄ :Yb@NaNdF ₄ :Yb	808	1525	Lifetime domain	Tumor biomarkers sensing	[33]
NaYbF ₄ :Er@NaYF ₄ & PbS QDs	980&808	1530&1600	Fluorescence lifetime	Tumor cells labeling	[91]
NaYF ₄ @NaYF ₄ :Nd@MY-1057	808	1060	Fluorescence lifetime	HCC tumor detection	[79]

First of all, the potential biotoxicity of nanoprobe induced by long-term retention often lacks systematic investigation. Currently, most researchers focus on the rational design of NIR-II fluorophores to achieve distinctive functions for specific application scenarios. However, large-sized and charged nanoprobe can be captured using the reticuloendothelial system and remain in live mammals for an extended period of time (1 month or longer) after biosensing, which may cause biosafety issues [20,95]. Therefore, designing long-circulating and renal-clearable NIR-II fluorophores for multichannel biosensing could be a way forward. Renal-clearable NIR-I nanosensors, such as golden nanoclusters or polyfluorophore nanoprobe, are applicable for in vivo detection and humoral diagnosis in

real time at a cellular level [96–98], which poses fewer concerns on the biosafety of these fluorophores during clinical implementation.

In addition to metabolizability, NIR-II fluorophores with long-wavelength emission in the NIR-IIb/NIR-IIc subwindow (NIR-IIb: 1500–1700 nm; NIR-IIc:1700–1880 nm) are favorable for deep-tissue biosensing with high resolution and contrast [99,100]. In terms of biosensing in the fluorescence-lifetime mode, fluorescent probes with responsiveness to stimulants in lifetime channels are still limited to the 950–1300 nm range [79,93]. Striking a delicate balance between the luminescence intensity and the lifetime of fluorescent probes is crucial in determining their effective use in practical applications. To meet this challenge, improving the luminescence intensity of NIR-IIb/NIR-IIc fluorophores while up- or downregulating the fluorescence lifetime might be the solution.

Last but not least, simplifying the components of NIR-II fluorophores can pave the way for clinical implementation. Hybrid nanoprobe remain the mainstream design for in vivo ratiometric quantification of various chemical substances (ROS, RNS, GSH, etc.), either in the form of chemical conjugation or physicochemical enclosure [54,62,64,66,73,77,79,93,101]. However, they may encounter dissociation or the release of components in physiological environments, posing significant biosafety risks. Our group has reported a single-component NIR-II fluorophore (LC-1250) for ratiometric fluorescence imaging of H₂O₂ to diagnose gastroenteritis with high sensitivity under physiological conditions (pH 1–2 in the stomach) [23], exemplifying that the ingenious design of organic dyes is key. Moreover, by endowing renal-clearable functionality, extending to longer emission wavelengths, or even incorporating portable devices [102], new fluorescent probes based on organic dyes could be developed for multichannel biosensing in future clinical practice.

Author Contributions: Conceptualization, writing—original draft preparation, F.R.; writing—review and editing, F.R., T.L. and T.Y.; visualization, G.C., C.L. and Q.W.; supervision, G.C., C.L. and Q.W.; project administration, Q.W.; funding acquisition, Q.W. All authors have read and agreed to the published version of the manuscript.

Funding: This research was funded by the National Natural Science Foundation of China (Grant Nos. 22201297, 21934007, 22127808, 22271308, 22174158, and 22177128); the National Key Research and Development Program (2021YFF0701804); the Chinese Academy of Sciences (Grant Nos. XDB36000000, ZDBS-LY-SLH021, and YJKYYQ20200036); the China Postdoctoral Science Foundation (Grant 2022M712327); the Science and Technology Project of Suzhou (Nos. SZS201904 and SJC2021001); the Natural Science Foundation of Jiangsu Province (Grant Nos. BK20222016, BE2022753, and BE2022745); and Jiangsu Funding Program for Excellent Postdoctoral Talent.

Institutional Review Board Statement: Not applicable.

Informed Consent Statement: Not applicable.

Data Availability Statement: There were no new data created or analyzed in this study. Data sharing does not apply to this article.

Acknowledgments: The authors thank researchers at Suzhou NIR-Optics Technology Co., Ltd., for their suggestions on the future development of in vivo NIR-II biosensing.

Conflicts of Interest: The authors declare no conflict of interest.

References

1. Li, C.; Wang, Q. Challenges and opportunities for intravital near-infrared fluorescence imaging technology in the second transparency window. *ACS Nano* **2018**, *12*, 9654–9659. [[CrossRef](#)]
2. Weissleder, R.; Pittet, M.J. Imaging in the era of molecular oncology. *Nature* **2008**, *452*, 580–589. [[CrossRef](#)]
3. Wang, K.; Du, Y.; Zhang, Z.; He, K.; Cheng, Z.; Yin, L.; Dong, D.; Li, C.; Li, W.; Hu, Z.; et al. Fluorescence image-guided tumour surgery. *Nat. Rev. Bioeng.* **2023**, *1*, 161–179. [[CrossRef](#)]
4. Andreou, C.; Weissleder, R.; Kircher, M.F. Multiplexed imaging in oncology. *Nat. Biomed. Eng.* **2022**, *6*, 527–540. [[CrossRef](#)]
5. Hu, Z.; Fang, C.; Li, B.; Zhang, Z.; Cao, C.; Cai, M.; Su, S.; Sun, X.; Shi, X.; Li, C.; et al. First-in-human liver-tumour surgery guided by multispectral fluorescence imaging in the visible and near-infrared-I/II windows. *Nat. Biomed. Eng.* **2020**, *4*, 259–271. [[CrossRef](#)] [[PubMed](#)]

6. Fan, Y.; Wang, S.; Zhang, F. Optical multiplexed bioassays for improved biomedical diagnostics. *Angew. Chem. Int. Ed.* **2019**, *58*, 13208–13219. [[CrossRef](#)] [[PubMed](#)]
7. Ma, T.; Hou, Y.; Zeng, J.; Liu, C.; Zhang, P.; Jing, L.; Shangguan, D.; Gao, M. Dual-ratiometric target-triggered fluorescent probe for simultaneous quantitative visualization of tumor microenvironment protease activity and pH in vivo. *J. Am. Chem. Soc.* **2018**, *140*, 211–218. [[CrossRef](#)] [[PubMed](#)]
8. Hong, G.S.; Antaris, A.L.; Dai, H.J. Near-infrared fluorophores for biomedical imaging. *Nat. Biomed. Eng.* **2017**, *1*, 0010. [[CrossRef](#)]
9. Chen, Y.; Wang, S.; Zhang, F. Near-infrared luminescence high-contrast in vivo biomedical imaging. *Nat. Rev. Bioeng.* **2023**, *1*, 60–78. [[CrossRef](#)]
10. Chen, G.; Cao, Y.; Tang, Y.; Yang, X.; Liu, Y.; Huang, D.; Zhang, Y.; Li, C.; Wang, Q. Advanced near-infrared light for monitoring and modulating the spatiotemporal dynamics of cell functions in living systems. *Adv. Sci.* **2020**, *7*, 1903783. [[CrossRef](#)]
11. Yang, H.; Huang, H.; Ma, X.; Zhang, Y.; Yang, X.; Yu, M.; Sun, Z.; Li, C.; Wu, F.; Wang, Q. Au-doped Ag₂Te quantum dots with bright NIR-IIb fluorescence for in situ monitoring of angiogenesis and arteriogenesis in a hindlimb ischemic model. *Adv. Mater.* **2021**, *33*, e2103953. [[CrossRef](#)] [[PubMed](#)]
12. Hong, G.S.; Robinson, J.T.; Zhang, Y.J.; Diao, S.; Antaris, A.L.; Wang, Q.B.; Dai, H.J. In vivo fluorescence imaging with Ag₂S quantum dots in the second near-infrared region. *Angew. Chem. Int. Ed.* **2012**, *51*, 9818–9821. [[CrossRef](#)] [[PubMed](#)]
13. Li, C.; Chen, G.; Zhang, Y.; Wu, F.; Wang, Q. Advanced fluorescence imaging technology in the near-infrared-II window for biomedical applications. *J. Am. Chem. Soc.* **2020**, *142*, 14789–14804. [[CrossRef](#)] [[PubMed](#)]
14. Sun, C.X.; Li, B.H.; Zhao, M.Y.; Wang, S.F.; Lei, Z.H.; Lu, L.F.; Zhang, H.X.; Feng, L.S.; Dou, C.R.; Yin, D.R.; et al. J-aggregates of cyanine dye for NIR-II in vivo dynamic vascular imaging beyond 1500 nm. *J. Am. Chem. Soc.* **2019**, *141*, 19221–19225. [[CrossRef](#)]
15. Yang, Y.; Sun, C.; Wang, S.; Yan, K.; Zhao, M.; Wu, B.; Zhang, F. Counterion-paired bright heptamethine fluorophores with NIR-II excitation and emission enable multiplexed biomedical imaging. *Angew. Chem. Int. Ed.* **2022**, *61*, e202117436.
16. Lu, L.; Li, B.; Ding, S.; Fan, Y.; Wang, S.; Sun, C.; Zhao, M.; Zhao, C.X.; Zhang, F. NIR-II bioluminescence for in vivo high contrast imaging and in situ ATP-mediated metastases tracing. *Nat. Commun.* **2020**, *11*, 4192. [[CrossRef](#)]
17. Bruns, O.T.; Bischof, T.S.; Harris, D.K.; Franke, D.; Shi, Y.; Riedemann, L.; Bartelt, A.; Jaworski, F.B.; Carr, J.A.; Rowlands, C.J.; et al. Next-generation in vivo optical imaging with short-wave infrared quantum dots. *Nat. Biomed. Eng.* **2017**, *1*, 0056. [[CrossRef](#)]
18. Du, Y.P.; Xu, B.; Fu, T.; Cai, M.; Li, F.; Zhang, Y.; Wang, Q.B. Near-infrared photoluminescent Ag₂S quantum dots from a single source precursor. *J. Am. Chem. Soc.* **2010**, *132*, 1470–1471. [[CrossRef](#)]
19. Zhu, X.; Liu, X.; Zhang, H.; Zhao, M.; Pei, P.; Chen, Y.; Yang, Y.; Lu, L.; Yu, P.; Sun, C.; et al. High-fidelity NIR-II multiplexed lifetime bioimaging with bright double interfaced lanthanide nanoparticles. *Angew. Chem. Int. Ed.* **2021**, *60*, 23545–23551. [[CrossRef](#)]
20. Ma, Z.; Wang, F.; Zhong, Y.; Salazar, F.; Li, J.; Zhang, M.; Ren, F.; Wu, A.M.; Dai, H. Cross-link-functionalized nanoparticles for rapid excretion in nanotheranostic applications. *Angew. Chem. Int. Ed.* **2020**, *59*, 20552–20560. [[CrossRef](#)]
21. Yu, G.T.; Luo, M.Y.; Li, H.; Chen, S.; Huang, B.; Sun, Z.J.; Cui, R.; Zhang, M. Molecular targeting nanoprobe with non-Overlap emission in the second near-infrared window for in vivo two-color colocalization of immune cells. *ACS Nano* **2019**, *13*, 12830–12839. [[CrossRef](#)] [[PubMed](#)]
22. Zhu, X.; Wang, X.; Zhang, H.; Zhang, F. Luminescence lifetime imaging based on lanthanide nanoparticles. *Angew. Chem. Int. Ed.* **2022**, *61*, e202209378. [[CrossRef](#)]
23. Li, T.; Cao, K.; Yang, X.; Liu, Y.; Wang, X.; Wu, F.; Chen, G.; Wang, Q. An oral ratiometric NIR-II fluorescent probe for reliable monitoring of gastrointestinal diseases in vivo. *Biomaterials* **2023**, *293*, 121956. [[CrossRef](#)] [[PubMed](#)]
24. Lan, Q.; Yu, P.; Yan, K.; Li, X.; Zhang, F.; Lei, Z. Polymethine molecular platform for ratiometric fluorescent probes in the second near-infrared window. *J. Am. Chem. Soc.* **2022**, *144*, 21010–21015. [[CrossRef](#)] [[PubMed](#)]
25. Yu, M.; Yang, X.; Zhang, Y.; Yang, H.; Huang, H.; Wang, Z.; Dong, J.; Zhang, R.; Sun, Z.; Li, C.; et al. Pb-doped Ag₂Se quantum dots with enhanced photoluminescence in the NIR-II window. *Small* **2021**, *17*, e2006111. [[CrossRef](#)]
26. Ortgies, D.H.; Tan, M.; Ximendes, E.C.; Del Rosal, B.; Hu, J.; Xu, L.; Wang, X.; Martin Rodriguez, E.; Jacinto, C.; Fernandez, N.; et al. Lifetime-encoded infrared-emitting nanoparticles for in vivo multiplexed imaging. *ACS Nano* **2018**, *12*, 4362–4368. [[CrossRef](#)]
27. Welsher, K.; Liu, Z.; Sherlock, S.P.; Robinson, J.T.; Chen, Z.; Daranciang, D.; Dai, H. A route to brightly fluorescent carbon nanotubes for near-infrared imaging in mice. *Nat. Nanotechnol.* **2009**, *4*, 773–780. [[CrossRef](#)]
28. Weidman, M.C.; Beck, M.E.; Hoffman, R.S.; Prins, F.; Tisdale, W.A. Monodisperse, air-stable PbS nanocrystals via precursor stoichiometry control. *ACS Nano* **2014**, *8*, 6363–6371. [[CrossRef](#)]
29. Hines, M.A.; Scholes, G.D. Colloidal PbS nanocrystals with size-tunable near-infrared emission: Observation of post-synthesis self-narrowing of the particle size distribution. *Adv. Mater.* **2003**, *15*, 1844–1849. [[CrossRef](#)]
30. Yang, H.; Li, R.; Zhang, Y.; Yu, M.; Wang, Z.; Liu, X.; You, W.; Tu, D.; Sun, Z.; Zhang, R.; et al. Colloidal alloyed quantum dots with enhanced photoluminescence quantum yield in the NIR-II window. *J. Am. Chem. Soc.* **2021**, *143*, 2601–2607. [[CrossRef](#)]
31. Naczynski, D.J.; Tan, M.C.; Zevon, M.; Wall, B.; Kohl, J.; Kulesa, A.; Chen, S.; Roth, C.M.; Riman, R.E.; Moghe, P.V. Rare-earth-doped biological composites as in vivo shortwave infrared reporters. *Nat. Commun.* **2013**, *4*, 2199. [[CrossRef](#)]
32. Johnson, N.J.; He, S.; Diao, S.; Chan, E.M.; Dai, H.; Almutairi, A. Direct evidence for coupled surface and concentration quenching dynamics in lanthanide-doped nanocrystals. *J. Am. Chem. Soc.* **2017**, *139*, 3275–3282. [[CrossRef](#)]

33. Fan, Y.; Wang, P.; Lu, Y.; Wang, R.; Zhou, L.; Zheng, X.; Li, X.; Piper, J.A.; Zhang, F. Lifetime-engineered NIR-II nanoparticles unlock multiplexed in vivo imaging. *Nat. Nanotechnol.* **2018**, *13*, 941–946. [[CrossRef](#)] [[PubMed](#)]
34. Bricks, J.L.; Kachkovskii, A.D.; Slominskii, Y.L.; Gerasov, A.O.; Popov, S.V. Molecular design of near infrared polymethine dyes: A review. *Dyes Pigments* **2015**, *121*, 238–255. [[CrossRef](#)]
35. Li, B.; Lu, L.; Zhao, M.; Lei, Z.; Zhang, F. An efficient 1064 nm NIR-II excitation fluorescent molecular dye for deep-tissue high-resolution dynamic bioimaging. *Angew. Chem. Int. Ed.* **2018**, *57*, 7483–7487. [[CrossRef](#)]
36. Cosco, E.D.; Spearman, A.L.; Ramakrishnan, S.; Lingg, J.G.P.; Saccomano, M.; Pengshung, M.; Arus, B.A.; Wong, K.C.Y.; Glasl, S.; Ntziachristos, V.; et al. Shortwave infrared polymethine fluorophores matched to excitation lasers enable non-invasive, multicolour in vivo imaging in real time. *Nat. Chem.* **2020**, *12*, 1123–1130. [[CrossRef](#)] [[PubMed](#)]
37. Antaris, A.L.; Chen, H.; Cheng, K.; Sun, Y.; Hong, G.S.; Qu, C.R.; Diao, S.; Deng, Z.X.; Hu, X.M.; Zhang, B.; et al. A small-molecule dye for NIR-II imaging. *Nat. Mater.* **2016**, *15*, 235–242. [[CrossRef](#)] [[PubMed](#)]
38. Bouit, P.A.; Aronica, C.; Toupet, L.; Guennic, B.L.; Andraud, C.; Maury, O. Continuous symmetry breaking induced by ion pairing effect in heptamethine cyanine dyes: Beyond the cyanine limit. *J. Am. Chem. Soc.* **2010**, *132*, 4328–4335. [[CrossRef](#)]
39. Luo, J.; Xie, Z.; Lam, J.W.; Cheng, L.; Chen, H.; Qiu, C.; Kwok, H.S.; Zhan, X.; Liu, Y.; Zhu, D.; et al. Aggregation-induced emission of 1-methyl-1,2,3,4,5-pentaphenylsilole. *Chem. Commun.* **2001**, *18*, 1740–1741. [[CrossRef](#)]
40. Li, Y.Y.; Liu, S.J.; Ni, H.W.; Zhang, H.; Zhang, H.Q.; Chuah, C.; Ma, C.; Wong, K.S.; Lam, J.W.Y.; Kwok, R.T.K.; et al. ACQ-to-AIE transformation: Tuning molecular packing by regioisomerization for two-photon NIR bioimaging. *Angew. Chem. Int. Ed.* **2020**, *59*, 12822–12826. [[CrossRef](#)]
41. Sheng, Z.; Guo, B.; Hu, D.; Xu, S.; Wu, W.; Liew, W.H.; Yao, K.; Jiang, J.; Liu, C.; Zheng, H.; et al. Bright aggregation-induced-emission dots for targeted synergetic NIR-II fluorescence and NIR-I photoacoustic imaging of orthotopic brain tumors. *Adv. Mater.* **2018**, *30*, e1800766. [[CrossRef](#)]
42. Li, Y.; Cai, Z.; Liu, S.; Zhang, H.; Wong, S.T.H.; Lam, J.W.Y.; Kwok, R.T.K.; Qian, J.; Tang, B.Z. Design of AIEgens for near-infrared IIb imaging through structural modulation at molecular and morphological levels. *Nat. Commun.* **2020**, *11*, 1255. [[CrossRef](#)] [[PubMed](#)]
43. Hong, Y.; Geng, W.; Zhang, T.; Gong, G.; Li, C.; Zheng, C.; Liu, F.; Qian, J.; Chen, M.; Tang, B.Z. Facile access to far-red fluorescent probes with through-space charge-transfer effects for in vivo two-photon microscopy of the mouse cerebrovascular system. *Angew. Chem. Int. Ed.* **2022**, *61*, e202209590. [[CrossRef](#)] [[PubMed](#)]
44. Qin, W.; Alifu, N.; Lam, J.W.Y.; Cui, Y.; Su, H.; Liang, G.; Qian, J.; Tang, B.Z. Facile synthesis of efficient luminogens with AIE features for three-photon fluorescence imaging of the brain through the intact skull. *Adv. Mater.* **2020**, *32*, e2000364. [[CrossRef](#)] [[PubMed](#)]
45. Qian, J.; Zhu, Z.; Leung, C.W.; Xi, W.; Su, L.; Chen, G.; Qin, A.; Tang, B.Z.; He, S. Long-term two-photon neuroimaging with a photostable AIE luminogen. *Biomed. Opt. Express* **2015**, *6*, 1477–1486. [[CrossRef](#)]
46. Mandal, A.K.; Sreejith, S.; He, T.H.; Maji, S.K.; Wang, X.J.; Ong, S.L.; Joseph, J.; Sun, H.D.; Zhao, Y.L. Three-photon-excited luminescence from unsymmetrical cyanostilbene aggregates: Morphology tuning and targeted bioimaging. *ACS Nano* **2015**, *9*, 4796–4805. [[CrossRef](#)]
47. Yao, C.; Chen, Y.; Zhao, M.; Wang, S.; Wu, B.; Yang, Y.; Yin, D.; Yu, P.; Zhang, H.; Zhang, F. A bright, renal-clearable NIR-II brush macromolecular probe with long blood circulation time for kidney disease bioimaging. *Angew. Chem. Int. Ed.* **2022**, *61*, e202114273. [[CrossRef](#)]
48. Wang, F.; Qu, L.; Ren, F.; Baghdasaryan, A.; Jiang, Y.; Hsu, R.; Liang, P.; Li, J.; Zhu, G.; Ma, Z.; et al. High-precision tumor resection down to few-cell level guided by NIR-IIb molecular fluorescence imaging. *Proc. Natl. Acad. Sci. USA* **2022**, *119*, e2123111119. [[CrossRef](#)]
49. Zhang, M.X.; Yue, J.Y.; Cui, R.; Ma, Z.R.; Wan, H.; Wang, F.F.; Zhu, S.J.; Zhou, Y.; Kuang, Y.; Zhong, Y.T.; et al. Bright quantum dots emitting at ~1600 nm in the NIR-IIb window for deep tissue fluorescence imaging. *Proc. Natl. Acad. Sci. USA* **2018**, *115*, 6590–6595. [[CrossRef](#)]
50. Ren, F.; Liu, H.H.; Zhang, H.; Jiang, Z.L.; Xia, B.; Genevois, C.; He, T.; Allix, M.; Sun, Q.; Li, Z.; et al. Engineering NIR-IIb fluorescence of Er-based lanthanide nanoparticles for through-skull targeted imaging and imaging-guided surgery of orthotopic glioma. *Nano Today* **2020**, *34*, 100905. [[CrossRef](#)]
51. Zhang, H.; Fu, P.; Liu, Y.; Zheng, Z.; Zhu, L.; Wang, M.; Abdellah, M.; He, M.; Qian, J.; Roe, A.W.; et al. Large-depth three-photon fluorescence microscopy imaging of cortical microvasculature on nonhuman primates with bright AIE probe in vivo. *Biomaterials* **2022**, *289*, 121809. [[CrossRef](#)]
52. He, M.; Li, D.; Zheng, Z.; Zhang, H.; Wu, T.; Geng, W.; Hu, Z.; Feng, Z.; Peng, S.; Zhu, L.; et al. Aggregation-induced emission nanoprobe assisted ultra-deep through-skull three-photon mouse brain imaging. *Nano Today* **2022**, *45*, 101536. [[CrossRef](#)]
53. Zheng, Z.; Zhang, H.; Cao, H.; Gong, J.; He, M.; Gou, X.; Yang, T.; Wei, P.; Qian, J.; Xi, W.; et al. Intra- and intermolecular synergistic engineering of aggregation-induced emission luminogens to boost three-photon absorption for through-skull brain imaging. *ACS Nano* **2022**, *16*, 6444–6454. [[CrossRef](#)] [[PubMed](#)]
54. Wang, T.; Chen, Y.; He, Z.; Wang, X.; Wang, S.; Zhang, F. Molecular-based FRET nanosensor with dynamic ratiometric NIR-IIb fluorescence for real-time in vivo imaging and sensing. *Nano Lett.* **2023**, *23*, 4548–4556. [[CrossRef](#)]
55. Wang, F.; Wan, H.; Ma, Z.; Zhong, Y.; Sun, Q.; Tian, Y.; Qu, L.; Du, H.; Zhang, M.; Li, L.; et al. Light-sheet microscopy in the near-infrared II window. *Nat. Methods* **2019**, *16*, 545–552. [[CrossRef](#)]

56. Dong, H.; Sun, L.D.; Yan, C.H. Local structure engineering in lanthanide-doped nanocrystals for tunable upconversion emissions. *J. Am. Chem. Soc.* **2021**, *143*, 20546–20561. [[CrossRef](#)]
57. Zhong, Y.; Ma, Z.; Zhu, S.; Yue, J.; Zhang, M.; Antaris, A.L.; Yuan, J.; Cui, R.; Wan, H.; Zhou, Y.; et al. Boosting the down-shifting luminescence of rare-earth nanocrystals for biological imaging beyond 1500 nm. *Nat. Commun.* **2017**, *8*, 737. [[CrossRef](#)] [[PubMed](#)]
58. Pei, P.; Chen, Y.; Sun, C.; Fan, Y.; Yang, Y.; Liu, X.; Lu, L.; Zhao, M.; Zhang, H.; Zhao, D.; et al. X-ray-activated persistent luminescence nanomaterials for NIR-II imaging. *Nat. Nanotechnol.* **2021**, *16*, 1011–1018. [[CrossRef](#)]
59. Wang, T.; Wang, S.; Liu, Z.; He, Z.; Yu, P.; Zhao, M.; Zhang, H.; Lu, L.; Wang, Z.; Wang, Z.; et al. A hybrid erbium(III)-bacteriochlorin near-infrared probe for multiplexed biomedical imaging. *Nat. Mater.* **2021**, *20*, 1571–1578. [[CrossRef](#)] [[PubMed](#)]
60. Bakueva, L.; Gorelikov, I.; Musikhin, S.; Zhao, X.S.; Sargent, E.H.; Kumacheva, E. PbS quantum dots with stable efficient luminescence in the NIR spectral range. *Adv. Mater.* **2004**, *16*, 926–929. [[CrossRef](#)]
61. McDonald, S.A.; Konstantatos, G.; Zhang, S.; Cyr, P.W.; Klem, E.J.; Levina, L.; Sargent, E.H. Solution-processed PbS quantum dot infrared photodetectors and photovoltaics. *Nat. Mater.* **2005**, *4*, 138–142. [[CrossRef](#)]
62. Yu, P.; Yan, K.; Wang, S.; Yao, C.; Lei, Z.; Tang, Y.; Zhang, F. NIR-II dyad-doped ratiometric nanosensor with enhanced spectral fidelity in biological media for in vivo biosensing. *Nano Lett.* **2022**, *22*, 9732–9740. [[CrossRef](#)] [[PubMed](#)]
63. Sun, Z.; Huang, H.; Zhang, R.; Yang, X.; Yang, H.; Li, C.; Zhang, Y.; Wang, Q. Activatable rare earth near-infrared-II fluorescence ratiometric nanoprobe. *Nano Lett.* **2021**, *21*, 6576–6583. [[CrossRef](#)] [[PubMed](#)]
64. Liao, N.; Su, L.; Zheng, Y.; Zhao, B.; Wu, M.; Zhang, D.; Yang, H.; Liu, X.; Song, J. In vivo tracking of cell viability for adoptive natural killer cell-based immunotherapy by ratiometric NIR-II fluorescence imaging. *Angew. Chem. Int. Ed.* **2021**, *60*, 20888–20896. [[CrossRef](#)] [[PubMed](#)]
65. Cui, D.; Li, J.; Zhao, X.; Pu, K.; Zhang, R. Semiconducting polymer nanoreporters for near-infrared chemiluminescence imaging of immunoactivation. *Adv. Mater.* **2020**, *32*, e1906314. [[CrossRef](#)]
66. Ramesh, A.; Kumar, S.; Brouillard, A.; Nandi, D.; Kulkarni, A. A nitric oxide (NO) nanoreporter for noninvasive real-time imaging of macrophage immunotherapy. *Adv. Mater.* **2020**, *32*, e2000648. [[CrossRef](#)]
67. Huang, Y.; Snuderl, M.; Jain, R.K. Polarization of tumor-associated macrophages: A novel strategy for vascular normalization and antitumor immunity. *Cancer Cell* **2011**, *19*, 1–2. [[CrossRef](#)]
68. Huang, Y.; Kim, B.Y.S.; Chan, C.K.; Hahn, S.M.; Weissman, I.L.; Jiang, W. Improving immune-vascular crosstalk for cancer immunotherapy. *Nat. Rev. Immunol.* **2018**, *18*, 195–203. [[CrossRef](#)]
69. Pittet, M.J.; Garris, C.S.; Arlauckas, S.P.; Weissleder, R. Recording the wild lives of immune cells. *Sci. Immunol.* **2018**, *3*, eaaq0491. [[CrossRef](#)]
70. Hao, X.; Li, C.; Zhang, Y.; Wang, H.; Chen, G.; Wang, M.; Wang, Q. Programmable chemotherapy and immunotherapy against breast cancer guided by multiplexed fluorescence imaging in the second near-infrared window. *Adv. Mater.* **2018**, *30*, e1804437. [[CrossRef](#)]
71. Lucero, M.Y.; Chan, J. Photoacoustic imaging of elevated glutathione in models of lung cancer for companion diagnostic applications. *Nat. Chem.* **2021**, *13*, 1248–1256. [[CrossRef](#)]
72. Tian, R.; Ma, H.; Zhu, S.; Lau, J.; Ma, R.; Liu, Y.; Lin, L.; Chandra, S.; Wang, S.; Zhu, X.; et al. Multiplexed NIR-II probes for lymph node-invaded cancer detection and imaging-guided surgery. *Adv. Mater.* **2020**, *32*, e1907365. [[CrossRef](#)] [[PubMed](#)]
73. Chen, Y.; Pei, P.; Yang, Y.; Zhang, H.; Zhang, F. Noninvasive early diagnosis of allograft rejection by a granzyme B protease responsive NIR-II bioimaging nanosensor. *Angew. Chem. Int. Ed.* **2023**, *62*, e202301696. [[CrossRef](#)] [[PubMed](#)]
74. Kantamneni, H.; Zevon, M.; Donzanti, M.J.; Zhao, X.; Sheng, Y.; Barkund, S.R.; McCabe, L.H.; Banach-Petrosky, W.; Higgins, L.M.; Ganesan, S.; et al. Surveillance nanotechnology for multi-organ cancer metastases. *Nat. Biomed. Eng.* **2017**, *1*, 993–1003. [[CrossRef](#)] [[PubMed](#)]
75. Duneton, C.; Winterberg, P.D.; Ford, M.L. Activation and regulation of alloreactive T cell immunity in solid organ transplantation. *Nat. Rev. Nephrol.* **2022**, *18*, 663–676. [[CrossRef](#)] [[PubMed](#)]
76. Cherry, C.; Maestas, D.R.; Han, J.; Andorko, J.I.; Cahan, P.; Fertig, E.J.; Garmire, L.X.; Elisseeff, J.H. Computational reconstruction of the signalling networks surrounding implanted biomaterials from single-cell transcriptomics. *Nat. Biomed. Eng.* **2021**, *5*, 1228–1238. [[CrossRef](#)]
77. Pei, P.; Hu, H.; Chen, Y.; Wang, S.; Chen, J.; Ming, J.; Yang, Y.; Sun, C.; Zhao, S.; Zhang, F. NIR-II ratiometric lanthanide-dye hybrid nanoprobe doped bioscaffolds for in situ bone repair monitoring. *Nano Lett.* **2022**, *22*, 783–791. [[CrossRef](#)]
78. Del Rosal, B.; Benayas, A. Strategies to overcome autofluorescence in nanoprobe-driven in vivo fluorescence imaging. *Small Methods* **2018**, *2*, 1800075. [[CrossRef](#)]
79. Zhao, M.; Li, B.; Wu, Y.; He, H.; Zhu, X.; Zhang, H.; Dou, C.; Feng, L.; Fan, Y.; Zhang, F. A tumor-microenvironment-responsive lanthanide-cyanine FRET sensor for NIR-II luminescence-lifetime in situ imaging of hepatocellular carcinoma. *Adv. Mater.* **2020**, *32*, e2001172. [[CrossRef](#)]
80. Becker, W. Fluorescence lifetime imaging—Techniques and applications. *J. Microsc.* **2012**, *247*, 119–136. [[CrossRef](#)]
81. Del Rosal, B.; Ortgies, D.H.; Fernandez, N.; Sanz-Rodriguez, F.; Jaque, D.; Rodriguez, E.M. Overcoming autofluorescence: Long-lifetime infrared nanoparticles for time-gated in vivo imaging. *Adv. Mater.* **2016**, *28*, 10188–10193. [[CrossRef](#)]
82. Gu, Y.; Guo, Z.; Yuan, W.; Kong, M.; Liu, Y.; Liu, Y.; Gao, Y.; Feng, W.; Wang, F.; Zhou, J.; et al. High-sensitivity imaging of time-domain near-infrared light transducer. *Nat. Photon.* **2019**, *13*, 525–531. [[CrossRef](#)]

83. Li, H.; Tan, M.; Wang, X.; Li, F.; Zhang, Y.; Zhao, L.; Yang, C.; Chen, G. Temporal multiplexed in vivo upconversion imaging. *J. Am. Chem. Soc.* **2020**, *142*, 2023–2030. [[CrossRef](#)]
84. Wu, L.; Jia, M.; Li, D.; Chen, G. Shell engineering on thermal sensitivity of lifetime-based NIR nanothermometers for accurate temperature measurement in murine internal liver organ. *Nano Lett.* **2023**, *23*, 2862–2869. [[CrossRef](#)] [[PubMed](#)]
85. Lu, Y.; Zhao, J.; Zhang, R.; Liu, Y.; Liu, D.; Goldys, E.M.; Yang, X.; Xi, P.; Sunna, A.; Lu, J.; et al. Tunable lifetime multiplexing using luminescent nanocrystals. *Nat. Photon.* **2013**, *8*, 32–36. [[CrossRef](#)]
86. Qiu, X.; Zhou, Q.; Zhu, X.; Wu, Z.; Feng, W.; Li, F. Ratiometric upconversion nanothermometry with dual emission at the same wavelength decoded via a time-resolved technique. *Nat. Commun.* **2020**, *11*, 4. [[CrossRef](#)] [[PubMed](#)]
87. Ribas, J.D.W. Cancer immunotherapy using checkpoint blockade. *Science* **2018**, *359*, 1350–1355. [[CrossRef](#)]
88. June, C.H.; O'Connor, R.S.; Kawalekar, O.U.; Ghassemi, S.; Milone, M.C. CAR T cell immunotherapy for human cancer. *Science* **2018**, *359*, 1361–1365. [[CrossRef](#)]
89. Bensch, F.; van der Veen, E.L.; Lub-de Hooge, M.N.; Jorritsma-Smit, A.; Boellaard, R.; Kok, I.C.; Oosting, S.F.; Schroder, C.P.; Hiltermann, T.J.N.; van der Wekken, A.J.; et al. (89)Zr-atezolizumab imaging as a non-invasive approach to assess clinical response to PD-L1 blockade in cancer. *Nat. Med.* **2018**, *24*, 1852–1858. [[CrossRef](#)]
90. Zou, W.; Wolchok, J.D.; Chen, L. PD-L1 (B7-H1) and PD-1 pathway blockade for cancer therapy: Mechanisms, response biomarkers, and combinations. *Sci. Transl. Med.* **2016**, *8*, 328rv4. [[CrossRef](#)]
91. Zhong, Y.; Ma, Z.; Wang, F.; Wang, X.; Yang, Y.; Liu, Y.; Zhao, X.; Li, J.; Du, H.; Zhang, M.; et al. In vivo molecular imaging for immunotherapy using ultra-bright near-infrared-IIb rare-earth nanoparticles. *Nat. Biotechnol.* **2019**, *37*, 1322–1331. [[CrossRef](#)] [[PubMed](#)]
92. Ma, X.; Zhang, M.J.; Wang, J.; Zhang, T.; Xue, P.; Kang, Y.; Sun, Z.J.; Xu, Z. Emerging biomaterials imaging antitumor immune response. *Adv. Mater.* **2022**, *34*, e2204034. [[CrossRef](#)] [[PubMed](#)]
93. Zhao, M.; Zhuang, H.; Zhang, H.; Li, B.; Ming, J.; Chen, X.; Chen, M. A LRET nanoplatform consisting of lanthanide and amorphous manganese oxide for NIR-II luminescence lifetime imaging of tumor redox status. *Angew. Chem. Int. Ed.* **2022**, *61*, e202209592. [[CrossRef](#)] [[PubMed](#)]
94. Chang, B.; Li, D.; Ren, Y.; Qu, C.; Shi, X.; Liu, R.; Liu, H.; Tian, J.; Hu, Z.; Sun, T.; et al. A phosphorescent probe for in vivo imaging in the second near-infrared window. *Nat. Biomed. Eng.* **2021**, *6*, 629–639. [[CrossRef](#)]
95. Liu, J.; Wang, P.; Zhang, X.; Wang, L.; Wang, D.; Gu, Z.; Tang, J.; Guo, M.; Cao, M.; Zhou, H.; et al. Rapid degradation and high renal clearance of Cu₃BiS₃ nanodots for efficient cancer diagnosis and photothermal therapy in vivo. *ACS Nano* **2016**, *10*, 4587–4598. [[CrossRef](#)]
96. He, S.; Cheng, P.; Pu, K. Activatable near-infrared probes for the detection of specific populations of tumour-infiltrating leukocytes in vivo and in urine. *Nat. Biomed. Eng.* **2023**, *7*, 281–297. [[CrossRef](#)]
97. Huang, J.; Chen, X.; Jiang, Y.; Zhang, C.; He, S.; Wang, H.; Pu, K. Renal clearable polyfluorophore nanosensors for early diagnosis of cancer and allograft rejection. *Nat. Mater.* **2022**, *21*, 598–607. [[CrossRef](#)]
98. Loynachan, C.N.; Soleimany, A.P.; Dudani, J.S.; Lin, Y.; Najer, A.; Bekdemir, A.; Chen, Q.; Bhatia, S.N.; Stevens, M.M. Renal clearable catalytic gold nanoclusters for in vivo disease monitoring. *Nat. Nanotechnol.* **2019**, *14*, 883–890. [[CrossRef](#)]
99. Wang, F.; Ren, F.; Ma, Z.; Qu, L.; Gourgues, R.; Xu, C.; Baghdasaryan, A.; Li, J.; Zadeh, I.E.; Los, J.W.N.; et al. In vivo non-invasive confocal fluorescence imaging beyond 1,700 nm using superconducting nanowire single-photon detectors. *Nat. Nanotechnol.* **2022**, *17*, 653–660. [[CrossRef](#)]
100. Chang, Y.; Chen, H.; Xie, X.; Wan, Y.; Li, Q.; Wu, F.; Yang, R.; Wang, W.; Kong, X. Bright Tm³⁺-based downshifting luminescence nanoprobe operating around 1800 nm for NIR-IIb and c bioimaging. *Nat. Commun.* **2023**, *14*, 1079. [[CrossRef](#)]
101. Zhao, M.; Wang, J.; Lei, Z.; Lu, L.; Wang, S.; Zhang, H.; Li, B.; Zhang, F. NIR-II pH sensor with a FRET adjustable transition point for in situ dynamic tumor microenvironment visualization. *Angew. Chem. Int. Ed.* **2021**, *60*, 5091–5095. [[CrossRef](#)] [[PubMed](#)]
102. Li, S.; Zhang, H.; Huang, Z.; Jia, Q. Spatially confining copper nanoclusters in porous ZrO₂ for fluorescence/colorimetry/smartphone triple-mode detection of metoprolol tartrate. *Biosens. Bioelectron.* **2023**, *231*, 115290. [[CrossRef](#)] [[PubMed](#)]

Disclaimer/Publisher's Note: The statements, opinions and data contained in all publications are solely those of the individual author(s) and contributor(s) and not of MDPI and/or the editor(s). MDPI and/or the editor(s) disclaim responsibility for any injury to people or property resulting from any ideas, methods, instructions or products referred to in the content.